Published in final edited form as:
IEEE Trans Biomed Eng. 2008 October ; 55(10): 2397–2406. doi:10.1109/TBME.2008.925693.

A Thermal Monitoring Sheet with Low Influence from Adjacent Waterbolus for Tissue Surface Thermometry during Clinical Hyperthermia

K. Arunachalam[*], **P.F. Maccarini**, and **P. R. Stauffer**
Radiation Oncology, Duke University Medical Center. 19196681980

Abstract

This paper presents a complete thermal analysis of a novel conformal surface thermometer design with directional sensitivity for real time temperature monitoring during hyperthermia treatments of large superficial cancer. The thermal monitoring sheet (TMS) discussed in this paper consists of a two-dimensional array of fiberoptic sensors embedded between two layers of flexible, low loss and thermally conductive printed circuit board (PCB) film. Heat transfer across all interfaces from the tissue surface through multiple layers of insulating dielectrics surrounding the small buried temperature sensor and into an adjacent temperature regulated water coupling bolus was studied using 3D thermal simulation software. Theoretical analyses were carried out to identify the most effective differential TMS probe configuration possible with commercially available flexible PCB materials, and to compare their thermal responses with omni-directional probes commonly used in clinical hyperthermia. A TMS sensor design that employs 0.0508m Kapton MTB® and 0.2032 mm Kapton HN® flexible polyimide films is proposed for tissue surface thermometry with low influence from the adjacent waterbolus. Comparison of the thermal simulations with clinical probes indicate the new differential TMS probe design to outperform in terms of both transient response and steady state accuracy in selectively reading the tissue surface temperature, while decreasing the overall thermal barrier of the probe between the coupling waterbolus and tissue surface.

Keywords

Thermal monitoring sheet; noninvasive thermometry; hyperthermia; surface temperature distribution measurement; thermal modeling; heat transfer

1. Introduction

The efficacy of moderate temperature hyperthermia combined with radiation has been demonstrated in numerous clinical studies over the past three decades [1-3] . Hyperthermia treatment of superficial tissue disease such as the chest wall recurrence of breast cancer has proven particularly beneficial, as demonstrated in several positive randomized clinical trials [4-6]. Although heat treatments have been delivered successfully with numerous microwave and ultrasound applicators, applicator size is frequently inadequate to treat the entire disease. In order to provide a larger effective heating pattern and accommodate tissue heterogeneity and irregularly shaped disease typical of chest wall recurrences, recent development efforts have concentrated on producing larger multi-element array applicators [7,8]. While a few multi-element array hyperthermia applicators are already available commercially [9-11], many

*(kavitha.arunachalam@duke.edu).

others have been developed for treating superficial tissue disease and are awaiting commercialization [12-24]. The common problem in administering treatments with these multi-element array heating devices is gaining sufficient real time feedback about the tissue temperature under each independently powered heat source to produce a more uniform heating of the lateral extent of the superficial target tissue. Without thermal feedback information to control each source, the effectiveness of array applicators is reduced to closer to a single aperture heat source of equivalent size. The typical use of up to 8 individual fiberoptic sensors or high resistance lead thermistors (for electromagnetic applicators) or thermocouples (for ultrasound applicators) in clinical hyperthermia systems is generally insufficient for identification of maximum and minimum temperatures under an applicator and thus inadequate for real-time control of multi-element array applicators that may have up to 32 independent heat sources [7,8]. A critical limitation common to all these multi-element array applicators is the lack of adequate thermometry measurements for feedback control of the heating elements.

The target tissue in superficial diseases like chestwall recurrence of breast carcinoma and plaque psoriasis generally extends 5-15mm beneath the tissue surface including the skin [8]. Clinical data suggest temperatures on the skin surface distribution as a good indicator of the underlying tissue temperature distribution within top 2-10 mm of the surface [8,25]. Theoretical study of 915 MHz microwave hyperthermia applicator indicates that peak temperatures occur 2-3 mm beneath the skin surface for practical waterbolus temperatures around 42°C [14]. These studies and practical limitations on the use of interstitial probes for large extent surface disease have led to the use of skin surface temperature measurements to monitor thermal dose and balance power radiated by the individual heating elements during hyperthermia treatments of superficial tissue disease. In a typical superficial disease hyperthermia treatment energy radiated by the heating device (microwaves or ultrasound) is coupled to the target tissue via a stable temperature controlled water bolus and the thermal dose delivered to the diseased tissue is controlled in real-time using omni-directional temperature probes taped to the skin surface. To obtain a more complete assessment of the tissue surface temperature, sensors are sometimes pulled manually inside thermal mapping catheters that are taped to the skin surface and temperature measurements recorded at 5-10 mm increments along the catheter. Though this procedure increases the number of measurement points, it generally produces a high density of points along each catheter for a small number of catheters since it is time consuming to complete each thermal map. In addition, temperature probes and thermal mapping catheters taped to a wet skin surface are prone to slipping from patient movement during treatment, resulting in uncertainty or errors in sensor position. With or without disease that may be breaking through the skin surface, the irregularly contoured anatomy of the human torso complicates alignment of multiple thermal mapping catheters that would be necessary to obtain a regularly spaced 2D grid of temperature measurements for real-time feedback power control of a multi-element array heat applicator. Due to their omni-directional thermal sensitivity, clinical probes (fiberoptic, thermistor or thermocouple) placed on tissue surface measure temperatures approximately midway between the true temperatures of the waterbolus and skin surface [25]. The plastic casing around the sensor that is necessary for a robust and reusable probe introduces a thermal barrier which impacts the speed and accuracy of temperature measurement. In addition to these drawbacks, the small amount of air surrounding the sensor inside thermal mapping catheters introduces further time delay and uncertainty to the temperature measurements.

The limitations of circular cross section clinical probes most commonly used for superficial tissue temperature monitoring provided the motivation to develop alternative thermometry devices. As a result, a prototype thermal monitoring sheet was constructed for real time surface temperature measurements. The design and construction of the initial prototype TMS sensor array which is evaluated in [26] are briefly reviewed in section 2.1. The transient and steady state thermal conduction equations used in the theoretical analysis to study the thermal response

of the TMS and other clinical probes at the interface of a layered media are presented in section 2.2. Section 2.3 presents the experimental validation of the thermal model analyzed using commercial 3D thermal simulation software. The identification of best performing TMS probe configuration of those possible with readily available flexible PCB materials is covered in section 2.4.1. Thermal models used to compare the performance of TMS probe configurations with commonly used circular cross section clinical probes are explained in section 2.4.2. Section 3.1 presents experimental validation of the thermal simulation software with prototype TMS sensor data. Simulation results for the identification of the most effective TMS probe configuration and performance comparison with the common clinical probes are presented in section 3.2. The outcome of the theoretical evaluation and implications of the accuracy of new TMS probes compared to circular cross section probes typically used for tissue surface temperature monitoring during superficial hyperthermia are discussed in section 4.

2. Methods

2.1 Conformal TMS Sensor Array Construction

A prototype TMS sensor array intended for monitoring tissue surface temperature distributions was developed in a research collaboration with IPITEK Inc (Carlsbad, CA, USA). The prototype TMS consists of a regularly spaced array of plastic fiberoptic probes securely trapped between two layers of thin polymer film. The need for the sensor array to conform closely to the skin surface over complex contoured anatomy led to the use of readily available flexible and thermally conductive Kapton HN® polyimide film used in PCB fabrication [27]. Microwave field perturbation studies conducted for four different diameter Teflon probes under a 915 MHz microwave antenna were used to select 250 μm diameter IPITEK electromagnetic field immune plastic fiberoptic probes [26]. Fig 1 shows the prototype 4×4 planar TMS sensor array with the fiberoptic sensors embedded between two Kapton HN® films of different thickness (L_1=100μm and L_2=175μm thick). The differential thickness (L_1<L_2) provides reduced thermal resistance to temperature measurements on one side of the sensor sheet. The spacing between sensors was chosen to match the center to center spacing of 16 heat sources in the commercial Microtherm and Sonotherm (Labthermics Technologies Inc, Champaign IL) planar array applicators. Each of the fiberoptic temperature probes inside the TMS sensor array is terminated with proprietary IPITEK fiberoptic connectors for data acquisition and calibration.

2.2 Theory

The transfer of thermal energy through multiple layers of dielectrics surrounding a temperature sensor located at the interface between two surfaces maintained at different temperatures was studied using the conduction heat equation [28],

$$-\nabla \cdot (k\nabla T(x,y,z,t)) + \rho c \frac{\partial T(x,y,z,t)}{\partial t} = 0; \quad (x,y,z) \in \Omega \quad \forall \quad t>0. \tag{1a}$$

subjected to the adiabatic boundary condition,

$$-k(\hat{n} \cdot \nabla T(x,y,z,t)) = 0; \quad (x,y,z) \in \partial\Omega, \quad \forall \quad t>0. \tag{1b}$$

In Eqn (1), T(x,y,z,t) is the spatial distribution of temperature at time instance, *t*; *k* is the material thermal conductivity; ρ is the material density; *c* is the specific heat capacity of the material; $\hat{n}$ is the surface normal; Ω defines the 3D computational domain and δΩ represents the computational boundary. At steady state, Eqns (1a) and (1b) reduce to the form,

$$-\nabla \cdot (k\nabla T(x,y,z)) = 0; \quad (x,y,z) \in \Omega \tag{2a}$$

$$-k(\hat{n} \cdot \nabla T) = 0; \quad (x,y,z) \in \partial\Omega \tag{2b}$$

Eqn (2a) is also known as the Fourier's law of heat conduction. Heat transfer inside the temperature probe was studied by solving Eqns (1) and (2) for appropriate thermal gradients across the probe. Thermal phenomena inside the tissue layer adjacent to the waterbolus-probe interface was studied using Pennes's bio-heat transfer equation,

$$-\nabla \cdot (k\nabla T(x,y,z,t)) + \rho c \frac{\partial T(x,y,z,t)}{\partial t} = -Q_b; \quad (x,y,z) \in \Omega, \quad \forall \quad t>0 \tag{3}$$

that accounts for thermal loss due to blood flow. The term, $Q_b \rho c\omega_b (T - T_a)$ in (3) denotes power loss due to blood perfusion inside the tissue at a rate, ω_b for the arterial blood temperature, $T_a = 37° C$. Thermal analyses presented in this paper were studied using 3D thermal simulation software (ePhysics, Ansoft Corp. Pittsburg, PA, USA).

2.3 Experimental Model Validation

Prior to simulating the TMS thermal problem, accuracy of the thermal solver was validated with corresponding experimental measurements of a prototype TMS sensor array. Fig 2a shows the experimental setup used to obtain temperature measurements from the 4×4 planar prototype TMS sensor array. A steep temperature gradient was maintained across a 0.125 mm thick Mylar film separation between two adjacent plexiglass waterbath chambers (each 10×15×15cm). Temperature inside the well-stirred waterbath chambers was controlled by circulating water through temperature controlled heat exchangers. The waterbath temperatures were measured with ±0.1°C accuracy using Physitemp thermocouple thermometers (BAT-10, Physitemp, Clifton, NJ, USA). The thicker Kapton side of the TMS prototype was taped securely to a 1.8 cm thick sheet of high density polystyrene (Dow Chemical, MI, USA) to insulate the back surface and the thinner Kapton side was placed above and in contact with the 32.1°C waterbath. After several minutes of equilibration, the TMS was slid swiftly across to the adjacent 40.1°C bath chamber. Real time temperature measurements from the individual fiberoptic sensors were acquired using IPITEK readout instrument connected to a personal computer.

A simplified TMS model with single embedded sensor was investigated as representative of the response of each sensor in the large 2D array. Fig 2b shows the computational geometry of the prototype TMS model sandwiched between the waterbath and polystyrene slab. In addition to the layers of dielectrics surrounding the sensor, the adhesive surrounding the round fiberoptic probe was also appropriately accommodated in the 3D TMS probe model. To mimic the experiment, the temperature of the waterbath (Ω_2) in Fig 2b was changed from 32.1°C to 40.1°C within 2 seconds (approximately the time required to slide the TMS over the adjacent waterbath). Steady state thermal simulation was carried out for the computational model in Fig 2b by solving Eqn (2) with $T(\Omega_1)$=29°C (Ω_1: room temperature) and $T(\Omega_2)$=32.1°C (Ω_2: waterbath). The steady state solution of the model was provided as the initial condition to the transient thermal problem. The transient model solved equation (1) for a step change in temperature inside the waterbath (Ω_2), i.e. T_2=32.1°C to 40.1°C within a time interval, Δt=2s. The material properties used in the simulation are listed in Table 1. The average temperature calculated inside the sensor volume was used to validate the steady state and transient solutions of the 3D thermal solver with the prototype TMS temperature measurements.

2.4 Thermal Models

2.4.1 Investigation of New TMS Probe Configuration—To avoid compatibility issues in bonding dissimilar films, investigation was limited to readily available Kapton films with thermal conductivities in the range of 0.12 - 0.45 W/m/K [28, 30].

2.4.1.1 Probe Thermal Sensitivity towards Tissue Surface: Tissue heating during clinical hyperthermia employs a waterbolus layer with temperature controlled distilled water (typically 42.5°C) between the heat applicator and tissue surface. The objective of this study was to identify a TMS probe configuration with lower thermal impedance on the side adjacent to the tissue surface and higher thermal isolation on the side facing away from the tissue such that the error (e_1) in temperature measured by the probe is minimal, where

$$e_1 = T_0 - t_{sensor}; \tag{4}$$

T_0 and T_{sensor} denote the tissue surface and sensor temperatures respectively. The thermal sensitivity of the buried fiberoptic temperature probe at the interface of a layered media at different temperatures depends on the thermal conduction capacitance (C_{thc}) and resistance (R_{thc}) of the surrounding TMS layers. The thermal resistance of a material with given cross sectional area increases with increase in material thickness and decrease in thermal conductivity, while the thermal capacitance is related to the specific heat capacity and material volume. Thus, TMS probe configurations with differential thermal conductivity and thickness Kapton films were studied for improved tissue surface temperature monitoring.

2.4.1.2 Probe Thermal Barrier between Tissue Surface and Waterbolus: The waterbolus between the heat applicator and target tissue helps produce more uniform tissue heating within the therapeutic range (41-44°C) under a hyperthermia array applicator, partially accommodating non-uniform power deposition and non-uniform tissue perfusion cooling. The waterbolus maintained at the mean therapeutic temperature of 42.5°C homogenizes spatial difference in tissue surface temperature during hyperthermia treatment by cooling hot spots (>44°C) and elevating temperature over regions with low sub-surface temperature (<41°C). Inserting a TMS sensor array between the waterbolus and skin surface adds a thermal barrier to the waterbolus which if excessive could compromise the ability of the waterbolus to regulate spatial inhomogeneities in tissue surface temperature during superficial hyperthermia treatment. In addition to the error (e_1) in reading temperature at an interface given by Eqn (4), a probe induced thermal barrier to the waterbolus was also considered in identifying the new TMS probe configuration. The relative changes in cooling (e_c) and heating (e_h) of superficial tissue by the 42.5°C waterbolus due to the finite thickness conformal TMS given by the expressions,

$$e_c = T^{TMS}\left(\Omega_{tissueSurf} | T_1=45; d=d_1\right) - T^{noTMS}\left(\Omega_{tissueSurf} | T_1=45; d=d_1\right) \tag{5a}$$

$$e_h = T^{TMS}\left(\Omega_{tissueSurf} | T_1=41; d=d_1\right) - T^{noTMS}\left(\Omega_{tissueSurf} | T_1=41; d=d_1\right) \tag{5b}$$

were used to quantify the thermal barrier of the TMS for a homogeneous temperature of T_1 at depth d_1 below the tissue surface (as might be anticipated from an external microwave or ultrasound heat source coupled to the tissue through a 42.5°C waterbolus). The expression, e_c in Eqn (5a) quantifies the relative change in tissue surface cooling by the 42.5°C waterbolus for a hot spot (T_1=45°C) at depth (d_1) beneath the tissue surface in the presence of the TMS.

The quantity, e_h in Eqn (5b) measures the relative change in elevating tissue surface temperature by the 42.5°C waterbolus over a region with low sub-surface tissue temperature (T_1=41°C) due to the presence of the TMS.

2.4.1.3 TMS Thermal Simulations: Simulations were carried out for a representative sub-section of the TMS array with single fiberoptic sensor embedded between two Kapton layers with the higher thermal conductivity (k_1=0.45 W/m/K) Kapton MTB film (L_1) on the side adjacent to the sensing surface and lower thermal conductivity (k_2=0.12 W/m/K) Kapton HN film (L_2) on the opposite surface. Prior analysis of field perturbation and probe self heating tests reported in [26] suggested a practical TMS layer thickness of 0.254mm (10 mil) to be acceptable. In the thermal analysis, Kapton film adjacent to the sensing surface (L_1) was set to 50.8μm to provide dimensional stability to the buried fiberoptic probes while conforming to contoured human torso, and to offer the least possible thermal impedance towards the sensing surface.

A parametric analysis of possible TMS probe configurations with differential thermal conductivity Kapton layers (k_1>k_2) was performed for varying thickness (L_2) of the low thermal conductivity Kapton HN layer over a range of 50.8-254μm. The 3D computational model with the TMS probe at the interface of two planar layered media shown in Fig 2b was used in the parametric study with the top surface at 42.5°C and bottom sensing surface at 37° C. The steady state thermal sensitivity of the TMS probe towards the 37°C surface was used to identify the possible TMS probe configurations. Figs 3a-b shows the layered computational model used to study the thermal isolation introduced by the finite thickness TMS probe towards the waterbolus. The single sensor TMS probe in Fig 3b is placed between the waterbolus sheet and muscle tissue with the 50.8 μm thick higher conductivity Kapton MTB on the tissue side. The material property and dimensions of the PVC waterbolus bag were adopted from the bolus bag currently used with the 32 element CMA heat applicators [29]. The relative change in tissue surface temperatures for a homogeneous temperature of T_1, 5mm beneath the muscle surface was calculated using Eqns (5a)-(5b) to study the thermal barrier of the TMS probe configuration to the waterbolus coupling layer.

2.4.2 Comparison of TMS Sensor with Common Clinical Thermometry Probes

2.4.2.1 Clinical Probe Models: Probe configurations most often used for monitoring superficial hyperthermia treatments include plastic core fiberoptic probes placed on the tissue surface either bare or inside a plastic thermal mapping catheter with a thin layer of air inside the catheter surrounding the probe. The steady state and transient thermal responses of the new TMS sensor configuration were compared to the following two representative thermometry probes that are commonly used for monitoring tissue surface temperatures in clinical hyperthermia: 1) 0.2 mm OD round cross section fiberoptic probes inside 0.5 mm OD polyethylene jacket with the phosphor sensor and pigmented Teflon protective coating at the probe tip (LMA 3100, Luxtron Corp. Santa Clara, CA, USA); and 2) LMA 3100 probe inside a 20 gauge Teflon catheter with 0.914mm ID and 1.524mm OD (BB311-20, Scientific Commodities Inc., Lake Havasu City, AZ). The cross sectional views of the layered 3D models in Figs 3c-d provide complete details of the clinical probes including the air trapped surrounding the sensor inside the catheter and catheter deformation under waterbolus pressure. The material properties used in the simulations are listed in Table 1.

2.4.2.2 Thermal Simulations: The steady state and transient behavior of the probes were studied using Eqns (1) and (2) to compare the ability of the probes to read tissue surface temperature accurately in space and time. The system response of the new TMS configuration and clinical probes were studied for a step change in temperature at the tissue surface given by,

$$T\left(\Omega_{tissueSurf}, t\right) = \begin{cases} 37°C; & t \le t_0 \\ 45°C; & t > t_0 + \Delta t_0 \end{cases} \quad (6)$$

with the deionized water inside the waterbolus maintained at 42.5 °C. The steady state solution at $t<t_0$ was provided as the initial condition to the transient thermal problem for the excitation in Eqn (6). The temperature inside the sensor volume calculated for the step change in thermal gradient across the probe was used to characterize the speed and time constant of the new TMS and clinical probes.

3. Simulation Results

3.1 Experimental Model Validation

Fig 4 shows the thermal response obtained for the computational model in Fig 2b where the prototype TMS was exposed to a step change in temperature of ~8°C. The average steady state temperatures measured by the TMS sensor sandwiched between the temperature regulated waterbath and polystyrene slab (thermal insulator) were observed to be 32.3°C and 39.8°C respectively before and after the step change. The thermal simulation is in agreement with the waterbath thermocouple readings of 32.1°C and 40.1°C. Comparison of the simulated TMS thermal response with experimental measurements in Fig 4 validates the thermal simulation software and the 3D probe model.

3.2 Identification of New TMS Probe Design

3.2.1 Thermal sensitivity towards Sensing Surface—Steady state thermal response of the differential thermal conductivity TMS probe was studied as a function of variable thickness (L_2) Kapton HN layer for a 5.5°C temperature gradient across the TMS ($L_1+L_2|_{max} \le 0.3$mm). Fig 5 compares the steady state temperature profiles along the transect AA′, which crosses through all layers of the TMS from the sensing surface at T_0=37 °C to the other side (42.5 ° C), via the sensor mid point (x=0, y=0) for a few selected TMS configurations. The graphs in Fig 5 clearly indicate the performance improvement obtained for TMS probe configurations with differential thickness and thermal conductivity Kapton layers. The thermal sensitivity error (e_1) decreases for TMS probe configurations with $L_2 >> L_1$. It can be observed that the average sensor temperature of 37.31°C calculated for the TMS model with L_2=254μm is the closest to the sensing surface (T_0=37°C) followed by the probe configuration with L_2=203.2μm. The differential TMS probe configuration, L_2=203.2μm with relatively low thermal sensing error (e_1) provides higher flexibility to contoured surface and low probe self heating as $L_1+L_2<0.3$mm.

3.2.2.Thermal Barrier towards Waterbolus—The thermal barrier induced by the differential TMS probe configuration with L_2=203.2μm was studied using the computational model in Fig 3b for tissue temperatures T_1=41°C and 45°C, 5mm beneath the muscle tissue. Steady state thermal analysis was carried out by solving the conduction heat Eqn (2) outside, and bio-heat transfer Eqn (3) inside the muscle tissue respectively for a blood perfusion rate, $\omega_b = 2.1e{-}3(1/s)$ [14]. Figs 6a-b compare the steady state temperature profiles at the waterbolus-muscle interface in the presence and absence of the new TMS probe configuration. The change in tissue surface cooling, e_c=0.48°C and heating, e_h=0.05°C calculated for the new TMS probe configuration indicate a low thermal isolation of the tissue from the waterbolus. The relatively small probe induced thermal barrier during hyperthermia treatment can be closely monitored by the new TMS probe and compensated by providing feedback control to the heating element. After investigating a number of TMS probe configurations, a TMS design with 50.8μm Kapton MTB (0.45 W/m/K) on the tissue/sensing side and 203.2μm Kapton HN

(0.12 W/m/K) on the waterbolus side was selected as an excellent compromise of thickness, durability, and thermal accuracy for tissue surface temperature monitoring with very small influence from the adjacent waterbolus.

3.3 Comparison with Clinical Probes

The thermal response of the new TMS and typical fiberoptic clinical probes were studied for a step change in temperature gradient across the probe. Fig 7a compares the average temperature inside the sensor volume calculated for the individual probes obtained by solving Eqns (1) and (6) for δt_0=10s. The steady state solution was fed as the initial condition for the transient problem. From the temperature curves in Fig 7a, it is evident that clinical probes 1 and 2 with additional plastic casing around the fiberoptic sensor respond slowly and are influenced by the 42.5°C waterbolus [25] unlike the differential TMS probe. A comparison of steady state 1D temperature profiles along the BB' transect in Fig 7b that passes through the multiple layers of the probe via the sensor midpoint at time $t<t_0$ clearly contrasts the directional sensitivity of the new TMS probe to the tissue surface with the omni-directional sensitivity of the clinical probes. In Figs 7a-b, the omni-directional thermal impedance experienced by the clinical probes towards the tissue surface and adjacent waterbolus impacts the steady state temperature accuracy and introduces time delay. The steady and transient characteristics of the new differential TMS probe clearly outperform the fiberoptic clinical probes commonly used for tissue surface temperature monitoring.

4. Discussion

This paper presents a theoretical study of the temperature sensing capabilities of several thermal monitoring approaches used to measure temperature distributions over large contoured surfaces. While probe configurations investigated in this work can be used to measure temperature of any surface, the specific application considered in this work is temperature monitoring of the tissue surface during clinical microwave hyperthermia treatments of large superficial tissue disease like chestwall recurrence of breast carcinoma. This study evaluates the relative speed and accuracy of surface temperature measurements made with several design options of a novel conformal sheet fiberoptic sensor array compared to circular cross section probes that are commonly used for clinical monitoring of microwave hyperthermia treatments. Possible design configurations based on commercially availability and fabrication feasibility were investigated with a goal to improve the thermal sensitivity of the buried fiberoptic sensors by reducing the effective thermal resistance and capacitance of one of the TMS layers without increasing the overall thermal impedance of the probe. The thermal gradient across the probe, from tissue surface (desired unknown temperature) through multiple layers of various insulating dielectrics surrounding a small buried temperature sensor, was studied using 3D thermal conduction model while heat transfer inside muscle tissue was solved using Penne's bio-heat transfer equation that includes provision for blood perfusion. The critical difference of this effort is that we are sensing only the temperature at the tissue surface and not at depth where other thermometry approaches must be used [8]. The 3D thermal simulation software, ePhysics used for the computational study was validated with experimental measurements in Fig 4. Unlike simulation data, experimental measurements are susceptible to errors from variation in material properties, and instrumentation and measurement noise. In interpreting the graphs in Fig 4, it should be noted that the good agreement between sensor measurement and waterbath temperature is primarily due to the presence of the polystyrene slab adjacent to the thin probe (<0.3mm). The very low thermal conductivity of the polystyrene slab (0.025 W/m/K) provides a controlled and repeatable experimental setup for model validation. The polystyrene slab is a thermal insulator which prevents heat flow from the well-stirred waterbath to the outer space across the probe, forcing the buried fiberoptic sensors inside the prototype TMS to read the bath temperature. The comparison between model and measurements in Fig

4 validates the 3D finite element probe model and the accuracy of the thermal solver. The close agreement between the prototype TMS sensor measurements in Fig 4 with thermocouple readings will deteriorate in the presence of heat transfer across the probe as seen in Fig 5.

Several TMS design configurations possible with readily available and easy to fabricate multilayer Kapton films were analyzed to improve the thermal sensitivity of the buried fiberoptic sensors to one preferred measurement side of the array. The error in reading the desired surface temperature (e_1) and tissue surface temperature heterogeneity caused by probe induced thermal barrier towards the waterbolus (e_c , e_h) calculated for the TMS configurations with L_1=50.8μm were used to identify the new TMS probe configuration. Comparison of the thermal gradient across the sensor in Fig 5 indicated that the thermal sensitivity of the TMS probe towards the 37°C surface improved with increase in thickness (L_2) of the low thermal conductivity Kapton HN film. The volume average sensor temperature of 37.31°C for L_2=254μm was the closest to the 37°C sensing surface followed by 31.37°C calculated for L_2=203.2μm. To provide flexibility and reduced probe self heating, a TMS probe configuration with L_2=203.2μm was chosen for surface temperature monitoring. Unlike the new TMS probe configuration with ratios of 4:1 in thermal conductivity and 4:1 in material thickness, the prototype TMS employs low thermal conductivity Kapton HN films with thickness ratio, 1.75:1. Thus, the thermal sensitivity error (e_1=−0.37°C) calculated for the new TMS probe configuration is much smaller than the prototype TMS (e_1=+1.4°C). The simulation results in Figs 6a-b for the new TMS probe configuration indicate the change in superficial tissue cooling and heating to be 0.48°C and 0.05°C respectively at clinically relevant tissue temperatures of 45°C and 41°C, 5mm beneath the tissue surface. The variation in tissue surface temperature calculated for ω_b=[2.15×10^{-4}, 2.1×10^{-3}](1/s) were observed to be e_c=[−0.31, 0.48]°C e_h= [0.14, 0.05]°C. This relatively small probe induced inhomogeneity in tissue surface temperature distribution could be closely monitored by the new differential TMS probe and compensated by changing the power radiated by the individual heating elements in the applicator array above the waterbolus. The new TMS probe configuration (L_1=0.0508 mm, L_2=0.2032 mm, k_1=0.45 W/m/K, k_2=0.12 W/m/K) with low thermal barrier towards the tissue surface and minimal overall increase in thermal isolation of tissue from the homogenizing effects of the water coupling bolus was chosen for tissue surface temperature monitoring.

The new TMS configuration was compared with common clinical probes to evaluate the transient and steady state response of the probes for a step change in thermal gradient at the interface between the waterbolus and tissue surface. The transient response curves in Fig 7a show that the directional sensing conformal TMS probe can more accurately monitor the true tissue surface temperature than the clinical probes. It should be noted that the 20 gauge Teflon catheter used in the computational model fits the bare plastic fiberoptic probe with small room for surrounding air gaps, and is much smaller than the 19-16 gauge catheters commonly used for tissue surface thermal mapping during hyperthermia treatments. Thus, the simulation results for clinical probes inside thermal mapping catheter analyzed in this comparative study presents an optimistic estimate of the clinical situation. The steady state temperature profiles in Fig 7b clearly indicate that clinical probes 1 and 2 with additional layers of thermal insulation (polyethylene jacket, mapping catheters and trapped air) present omni-directional thermal impedance to the buried fiberoptic sensor unlike the new TMS probe with differential thickness and thermal conductivity Kapton layers.

Table 2 lists the steady state thermal sensitivity error (e_1), and transient response (dT/dt) calculated for the new TMS and clinical probes from the curves in Fig 7b. The values in Table 2 indicate that a round cross section fiberoptic probe inside a thermal mapping catheter responds the slowest with the largest error (~2°C) in reading the tissue surface temperature due to additional plastic insulation and air surrounding the sensor. The protective plastic coating around the bare clinical probe provides an omni-directional thermal barrier towards the

phosphor sensor resulting in ~1.5°C error in tissue surface measurement. Consider that the tissue surface temperatures read by the new TMS and clinical probes are approximately 43.5° C and 42°C respectively, an error of 1.5°C measured by the clinical probe during the entire hyperthermia treatment will result in two fold error in the calculation of cumulative equivalent minutes thermal dose delivered to the target tissue given by [4],

$$CEM43T_{90}=\sum_{i=0}^{N} R^{43-T_{90i}}\Delta t. \tag{7}$$

In (7), R=1/2 for T_{90i}>43°C and R=1/4 for T_{90i}<43°C; $T90_i$ is the 90th percentile of the surface temperature measurements at the i^{th} time instant and the summation is carried out over the entire hyperthermia treatment duration of N minutes (typically, N=60 minutes). The plastic probes inside thermal mapping catheters that are widely used for invasive thermometry are less suited for superficial tissue temperature monitoring due to the omni-directional thermal sensitivity of the round cross section sensors. When these round probes are taped to the skin surface, they are prone to alignment and positioning errors which generally yield irregularly spaced 2D temperature distributions that are significantly influenced by bolus pressure and surface texture (i.e. relative hardness and irregularity of the skin and bolus membrane surfaces). The choice of thinner Kapton MTB film on the tissue side reduced the effective thermal resistance and capacitance of the embedded fiberoptic sensors in reading the desired unknown tissue surface temperature while a thicker Kapton HN film on the back side adjacent to the waterbolus had a reverse thermal effect, decoupling TMS sensor response from the 42.5°C waterbolus. The thermal resistance and capacitance experienced by the phosphor sensor at the probe tip, surrounded by layers of dielectrics calculated for the new TMS and clinical probes are listed in Table 2. The thermal resistance and capacitances were calculated for a unit long Phosphor sensor where r_i and a_i are the thickness and cross sectional area of the i_{th} cylindrical layer surrounding the sensor with material density, ρ_i ; thermal conductivity, k_i and specific heat capacity, c_i. The thermal impedance values in Table 2 indicate that round cross section clinical probes provide omni-directional thermal impedance to the sensor unlike the new differential TMS probe configuration. The new differential TMS probe configuration with a ratio of approximately 4:1 and 7:1 in thermal resistance and capacitance respectively offers the most directional thermal sensitivity for tissue surface temperature monitoring. Overall, the steady state and transient characteristics of the probes summarized in Table 2 and Figs 7a-b indicate that the new TMS probe configuration outperforms the circular cross section clinical probes and the previously developed prototype TMS for accurate monitoring of tissue surface temperature.

The new conformal TMS probe with a fixed array of embedded fiberoptic temperature sensors yield surface temperature distributions across large contoured tissue at regular spacing. The 2D thermal maps from high density TMS sensor arrays should enable improved monitoring and control of the multi-element hyperthermia array applicators. Improved surface thermometry should encourage increased utilization of the recently designed superficial hyperthermia applicators with increased levels of adjustability.

5. Conclusion

A novel conformal thermal monitoring sheet is investigated for applications requiring fast and accurate characterization of surface temperature distributions over large tissue surfaces overlying contoured anatomy. Parametric analyses of transient and steady state thermal simulations for thermal gradients across complex multilayered interfaces helped identify a clinically practical conformal thermal monitoring sheet sensor design. The new differential TMS design with a ratio of 4:1 in thermal conductivity and 4:1 in material thickness enabled

fast and accurate monitoring of tissue surface temperatures while adding low thermal barrier between the tissue surface and water coupling bolus. The speed and accuracy of the new TMS probe configuration with approximately 4:1 in thermal resistance and 7:1 in thermal capacitance across the buried fiberoptic sensor outperformed the circular cross section fiberoptic probes commonly used for clinical monitoring of microwave hyperthermia treatments. The conformability and directional thermal sensitivity to tissue surface while maintaining low overall thermal barrier between the target tissue and temperature-equalizing waterbolus demonstrate the new TMS probe configuration as the most appropriate thermometry design for tissue surface temperature monitoring in superficial hyperthermia treatments.

Acknowledgements

This effort was supported by NIH Grants R43-AR51278, R44-CA104061 and RO1-CA70761, as well as generous software support from Ansoft Corp. The authors would also like to express their appreciation of efforts by collaborators at UCSF Medical Center (Titania Juang and Daniel Neuman) and IPITEK Inc. (Dave Schafsma, John Rozanski, Doug Bonnell, Rick Forber and Cel Gaeta) in the development of the prototype TMS.

References

1. Sneed, PK., et al. Hyperthermia. In: Leibel, SA.; Phillips, TL., editors. Textbook of Radiation Oncology. W B Saunders Co.; Philadelphia: 1998. p. 1241-62.
2. Dewhirst, MW., et al. Hyperthermia. In: Kufe, D., et al., editors. Cancer Medicine. Decker; Hamilton BC: 2003. p. 623-36.
3. Seegenschmiedt, MH.; Fessenden, P.; Vernon, CC. Thermoradiotherapy and thermochemotherapy: volume 2, clinical applications. Springer-Verlag; Berlin, New York: 1996.
4. Jones EL, et al. Randomized trial of hyperthermia and radiation for superficial tumors. J Clin Oncol 2005;23(13):3079–85. [PubMed: 15860867]
5. Vernon CC, et al. Radiotherapy with or without hyperthermia in the treatment of superficial localized breast cancer: results from five randomized controlled trials. International Collaborative Hyperthermia Group. Int J Radiat Oncol Biol Phys 1996;35(4):731–44. [PubMed: 8690639]
6. Kapp DS. Efficacy of adjuvant hyperthermia in the treatment of superficial recurrent breast cancer: confirmation and future directions. International Journal of Radiation Oncology, Biology and Physics 1996;35(5):1117–21.
7. Stauffer PR. Evolving technology for thermal therapy of cancer. International Journal of Hyperthermia 2005;21(8):731–744. [PubMed: 16338856]
8. Stauffer, PR. Thermal therapy techniques for skin and superficial tissue disease. In: Ryan, TP., editor. A critical review, matching the energy source to the clinical need. SPIE Optical Engineering Press; Bellingham WA: 2000. p. 327-67.
9. Diederich CJ, Stauffer PR. Pre-clinical evaluation of a microwave planar array applicator for superficial hyperthermia. International Journal of Hyperthermia 1993;9:227–246. [PubMed: 8468507]
10. Samulski TV, et al. Clinical experience with a multi-element ultrasonic hyperthermia system: analysis of treatment temperatures. International Journal of Hyperthermia 1990;6(5):909–922. [PubMed: 2250116]
11. Johnson JE, et al. Evaluation of a dual arm archimedian spiral array for microwave hyperthermia. International Journal of Hyperthermia 2006;22(6):475–490. [PubMed: 16971368]
12. Lamaitre G, et al. SAR characteristics of three types of contact flexible microstrip applicators for superficial hyperthermia. International Journal of Hyperthermia 1996;12(2):255–69. [PubMed: 8926393]
13. Lee ER, et al. Body conformable 915 MHz microstrip array applicators for large surface area hyperthermia. IEEE Transactions on Biomedical Engineering 1992;39(5):470–483. [PubMed: 1526638]

14. Rossetto F, Diederich CJ, Stauffer PR. Thermal and SAR characterization of multielement dual concentric conductor microwave applicators for hyperthermia, a theoretical investigation. Medical Physics 2000;27(4):745–53. [PubMed: 10798697]
15. Sherar MD, et al. A variable microwave array attenuator for use with single-element waveguide applicators. International Journal of Hyperthermia 1994;10(5):723–731. [PubMed: 7806927]
16. Stauffer, PR., et al. Proc. of SPIE. SPIE Press; San Jose: 2007. Progress on Conformal Microwave Array Applicators for Heating Chestwall Disease.
17. Underwood HR, et al. A multi-element ultrasonic hyperthermia applicator with independent element control. International Journal of Hyperthermia 1987;3:257–267. [PubMed: 3655439]
18. Rietveld PJM, et al. Quantitative evaluation of 2*2 arrays of Lucite cone applicators in flat layered phantoms using Gaussian-beam-predicted and thermographically measured SAR distributions. Physics in Medicine and Biology 1998;43(8):2207–20. [PubMed: 9725599]
19. Novak P, et al. SURLAS: a new clinical grade ultrasound system for sequential or concomitant thermoradiotherapy of superficial tumors: applicator description. Medical Physics 2005;32(1):230–40. [PubMed: 15719974]
20. Hand, JW., et al. Current sheet applicator arrays for superficial hyperthermia. In: Gerner, E.; Cetas, T., editors. Hyperthermic Oncology 1992. Vol. vol. 2. Arizona Board of Regents; Tucson: 1993. p. 193-7.
21. Gopal MK, et al. Current sheet applicator arrays for superficial hyperthermia of chestwall lesions. International Journal of Hyperthermia 1992;8(2):227–240. [PubMed: 1573312]
22. Samulski TV, et al. Spiral microstrip hyperthermia applicators: technical design and clinical performance. International Journal of Radiation Oncology, Biology, Physics 1990;18(1):233–42.
23. Lee WM, et al. Assessment of the performance characteristics of a prototype 12-element capacitive contact flexible microstrip applicator (CFMA-12) for superficial hyperthermia. Int J Hyperthermia 2004;20(6):607–24. [PubMed: 15370817]
24. Stauffer, PR., et al. Proc. of SPIE. SPIE Press; San Jose: 2005. Progress on system for applying simultaneous heat and brachytherapy to large-area surface disease.
25. Lee ER, et al. Influence of water bolus temperature on measured skin surface and intradermal temperatures. International Journal of Hyperthermia 1994;10(1):59–72. [PubMed: 8144989]
26. Arunachalam K, et al. Performance evaluation of a conformal thermal monitoring sheet (TMS) sensor array for measurement of surface temperature distributions during superficial hyperthermia treatments. submitted to International Journal of Hyperthermia. 2007
27. DuPontTM, *DuPont™ Kapton® HN polyimide film - Technical Data Sheet*, DuPont™
28. Incropera, FP., et al. Vol. 6 ed. Wiley; 2006. Fundamentals of Heat and Mass Transfer.
29. Juang T, et al. Multilayer conformal applicator for microwave heating and brachytherapy treatment of superficial tissue disease. International Journal of Hyperthermia 2006;22(7):527–44. [PubMed: 17079212]

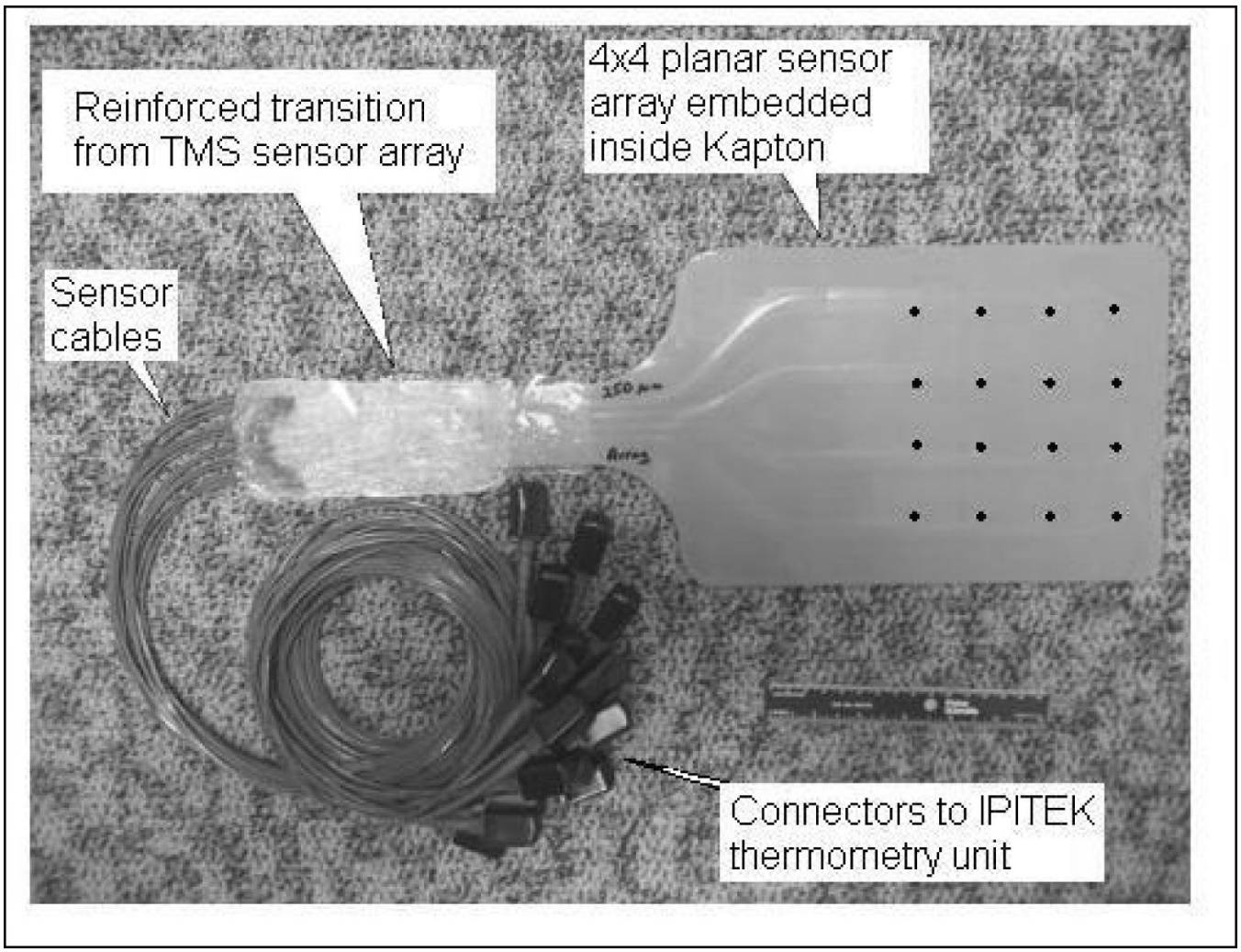

Fig 1.
Prototype TMS 4′4 fiberoptic sensor array with fiberoptic cabling and reinforced transition region for connection to the external IPITEK readout electronics. The black dots superimposed on the TMS indicate fiberoptic sensor locations.

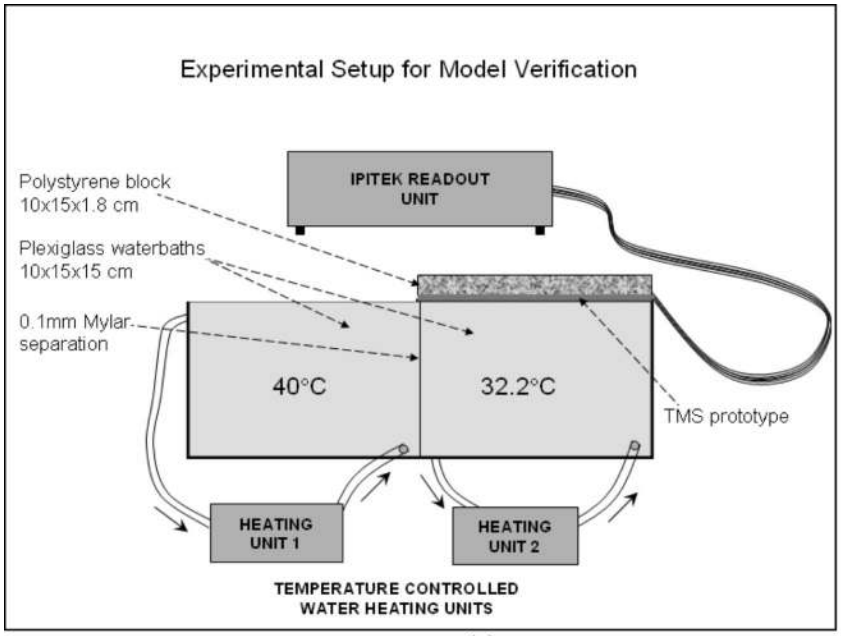

(a)

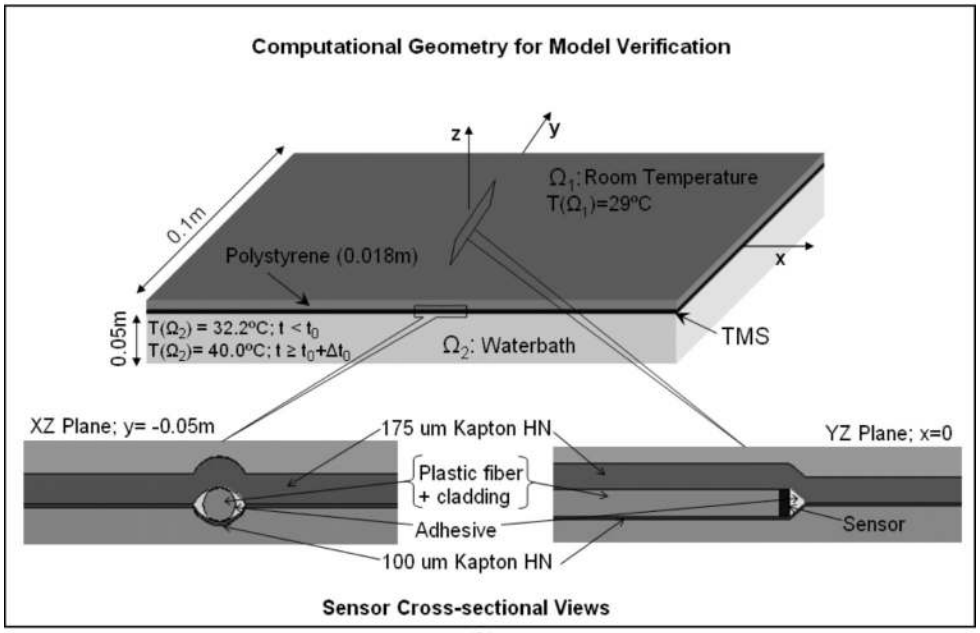

(b)

Fig 2.

Experimental model validation (a) Experimental setup of the temperature controlled dual chamber waterbath with prototype TMS sensor array taped to polystyrene sheet (thermal insulator) (b) 3D computational geometry for model validation with zoomed in views of the prototype TMS probe with single buried IPITEK fiberoptic sensor (240μm dia core and 250μm dia cladding).

Computational Geometry for Surface Monitoring Probe Comparison

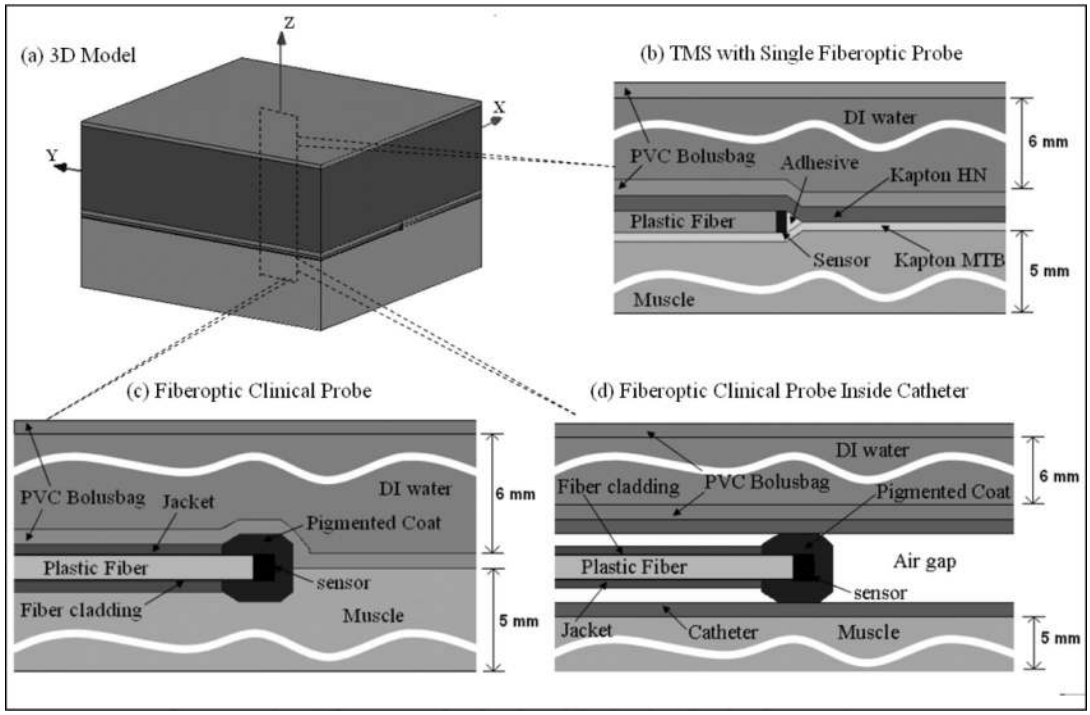

Fig 3.

Computational models of tissue surface monitoring probes (a) Multi-layered computational model of a clinical probe at the interface between muscle tissue and water coupling bolus as in superficial hyperthermia treatment; Cross sectional views of (b) TMS probe with 250μm dia Ipitek fiberoptic probe sandwiched between 50.8μm (L1) Kapton MTB on tissue side and Kapton HN (L_2) on bolus side (c) 200μm dia plastic fiberoptic probe inside 0.5mm OD polyethylene casing (Teflon PFA jacket) with 0.75mm OD protective Teflon coating (d) fiberoptic probe in Fig 3c inside 20 gauge Teflon catheter with 0.914mm ID and 1.524mm OD. For all cases, waterbolus thickness=6mm; PVC bolus bag thickness=0.3048mm (12mil); muscle thickness=5mm; computational model width=50mm and breadth=50mm.

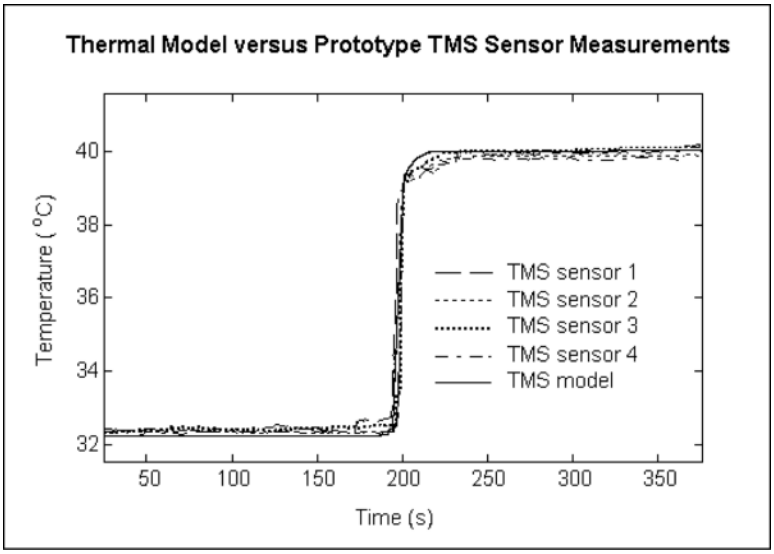

Fig 4.

Experimental validation of 3D thermal simulation analyzed using ePhysics software. Comparison of the volume average sensor temperature calculated for the single sensor prototype TMS model in Fig 2b with experimental measurements for a step change in waterbath temperature.

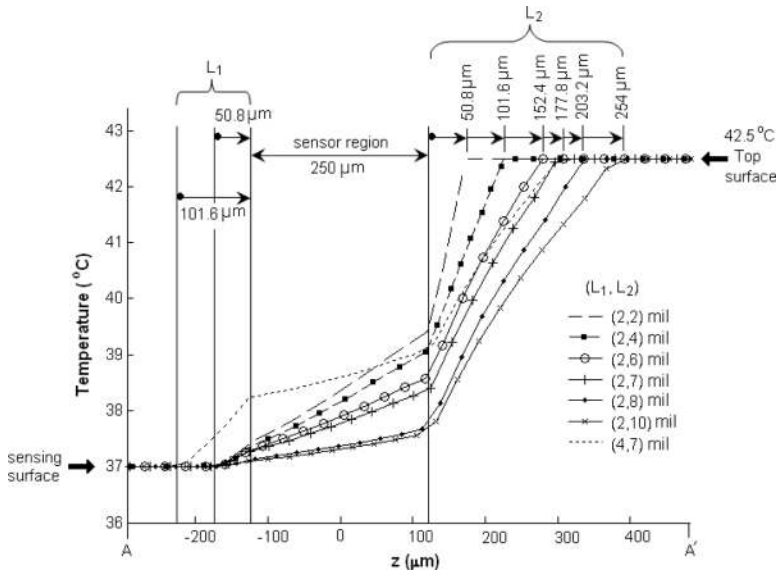

Fig 5.

Comparison of steady state temperature profiles through the cross section of several differential TMS probe configurations as a function of the thickness of the Kapton HN layer (L_2), with the TMS probe sandwiched between the 37°C sensing surface and 42.5°C top surface; 1mil=25.4µm.

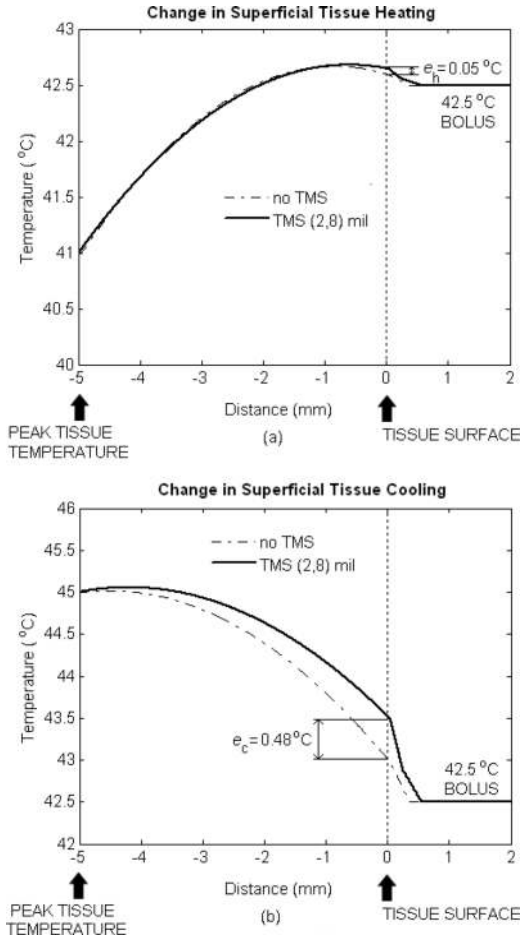

Fig 6.

Comparison of the steady state temperature along the z-axis of the layered tissue model in the presence and absence of the new TMS probe with L_1=50.8μm, L_2=203.2μm, k_1=0.45W/m/K and k_2=0.12W/m/K for a homogeneous tissue temperature of T_1°C, 5mm below muscle tissue. The relative change in tissue surface temperature calculated over a region with subsurface temperature: (a) below desired therapeutic temperature (T_1=41°C); and (b) above desired therapeutic temperature (T_1=45°C).

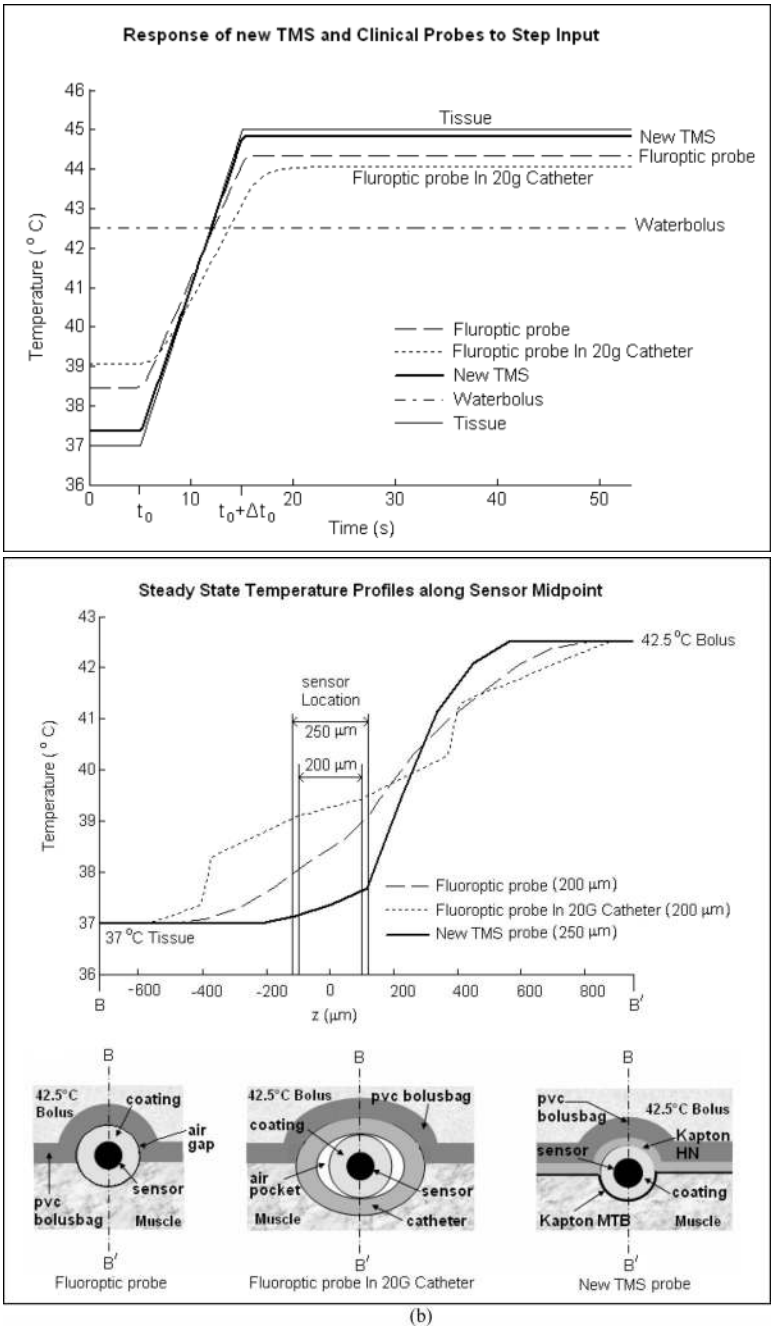

Fig 7.

Comparison of the new TMS probe configuration with clinical probes for a step change in temperature gradient across the probe; (a) Average temperature calculated inside the sensor volume for a step change in tissue surface temperature (b) Steady state temperature profiles through the sensor depicting the omni-directional thermal sensitivity of existing round cross section clinical probes and the directional sensitivity of the new TMS probe. Note that commonly used clinical probes located inside a thermal mapping catheter have the slowest transient response and largest error in reading tissue surface temperature.

Table 1

Material properties used in the thermal simulations [28, 30-34].

Materials	Density (Kg/m^3)	Thermal conductivity W/m/C)	Specific heat capacity (J/Kg/C)
Water	1000	0.6	4200
Kapton HN	1090	0.12	1420
Kapton MTB	1090	0.45	1420
Fiber core	1200	0.19	1390
Fiber cladding	1000	0.3	1500
Phosphor sensor	2100	0.81	210
Polyethylene Jacket	2150	0.27	1050
Polystyrene	45	0.025	2000
Teflon	2150	0.21	1100
Muscle	970	0.50	3514
Air	1.18	0.03	1006
PVC	1300	0.29	1500

Table 2

Summary of steady state and thermal responses, and thermal impedances calculated for the new differential TMS probe configuration and circular cross section fiberoptic probes used in clinical hyperthermia for tissue surface temperature monitoring. The thermal resistance and capacitances are calculated for a unit long phosphor sensor at the probe tip [29].

Probe Models	Thermal sensitivity error, e_1 (C)		$\left[\frac{dT^{muscle}}{dt} - \frac{dT^{sensor}}{dt}\right]^*$ (C/s)	Thermal resistance towards: $\sum_i \frac{\ln(r_{i+1}/r_i)}{2\pi k_i}$ [29]			Thermal capacitance towards: $\sum_i \rho_i a_i c_i$ [29]		
	T_{muscle}=37°C	T_{muscle}=45°C		Tissue, Rt_t (mC/W)	Bolus, R_b (mC/W)	$\frac{R_b}{R_t}$	Tissue, C_t (J/C/m)	Bolus, C_b (J/C/m)	$\frac{C_b}{C_t}$
bare plastic probe	1.46	−0.67	−0.25	2.60E3	2.60E3	1:1	3.60E-4	3.60E-4	1:1
bare probe in 20Gauge catheter	2.07	−0.94	−0.47	7.88E3	7.88E3	1:1	1.39E-3	1.39E-3	1:1
TMS probe	0.36	−0.16	−0.07	5.83E2	4.14E3	1:7	4.00E-5	1.50E-4	1:4

IEEE Trans Biomed Eng. Author manuscript; available in PMC 2009 October 1.